Near-Atomic Three-Dimensional Mapping for Site-Specific Chemistry of 'Superbugs'

Vahid R. Adineh,[†] Ross K. W. Marceau,[‡] Tony Velkov,[§] Jian Li,[||] and Jing Fu[*,†,⊥]

[†]Department of Mechanical and Aerospace Engineering, Monash University, Clayton, Victoria 3800, Australia

[‡]Institute for Frontier Materials, Deakin University, Geelong, Victoria 3216, Australia

[§]Drug Delivery, Disposition and Dynamics, Monash Institute of Pharmaceutical Sciences, Monash University, Parkville, Victoria 3052, Australia

[||]Monash Biomedicine Discovery Institute, Department of Microbiology, Monash University, Clayton, Victoria 3800, Australia

[⊥]ARC Centre of Excellence for Advanced Molecular Imaging, Monash University, Clayton, Victoria 3800, Australia

S *Supporting Information*
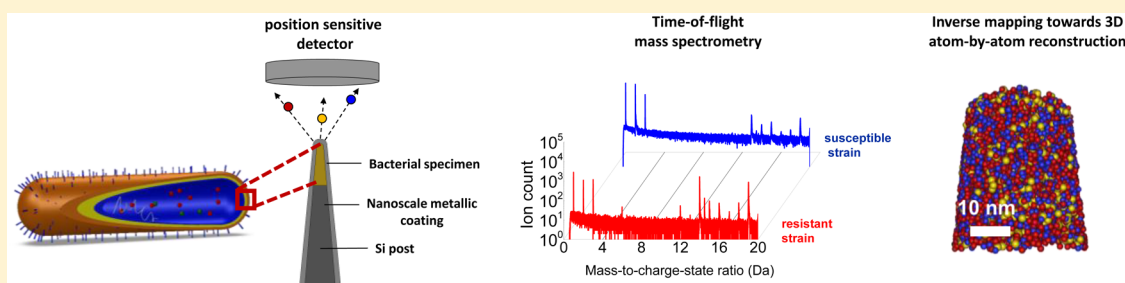
ABSTRACT: Emergence of multidrug resistant Gram-negative bacteria has caused a global health crisis and last-line class of antibiotics such as polymyxins are increasingly used. The chemical composition at the cell surface plays a key role in antibiotic resistance. Unlike imaging the cellular ultrastructure with well-developed electron microscopy, the acquisition of a high-resolution chemical map of the bacterial surface still remains a technological challenge. In this study, we developed an atom probe tomography (APT) analysis approach to acquire mass spectra in the pulsed-voltage mode and reconstructed the 3D chemical distribution of atoms and molecules in the subcellular domain at the near-atomic scale. Using focused ion beam (FIB) milling together with micromanipulation, site-specific samples were retrieved from a single cell of *Acinetobacter baumannii* prepared as needle-shaped tips with end radii less than 60 nm, followed by a nanoscale coating of silver in the order of 10 nm. The significantly elevated conductivity provided by the metallic coating enabled successful and routine field evaporation of the biological material, with all the benefits of pulsed-voltage APT. In parallel with conventional cryo-TEM imaging, our novel approach was applied to investigate polymyxin-susceptible and -resistant strains of *A. baumannii* after treatment of polymyxin B. Acquired atom probe mass spectra from the cell envelope revealed characteristic fragments of phosphocholine from the polymyxin-susceptible strain, but limited signals from this molecule were detected in the polymyxin-resistant strain. This study promises unprecedented capacity for 3D nanoscale imaging and chemical mapping of bacterial cells at the ultimate 3D spatial resolution using APT.

KEYWORDS: *Cell imaging, atom probe tomography, nanoscale chemical mapping, drug resistance, polymyxin*

Infections caused by 'superbugs', extremely antibiotic resistant bacteria, represent a significant global health problem, and it is estimated that antimicrobial resistant infections will kill one person every three seconds by 2050.[1] Based on the ongoing studies on antibiotic resistance, a wide range of biochemical and physiological mechanisms have been proposed and debated.[2] The differences between the chemical composition and structure of susceptible and resistant strains are considered to carry the fundamental information on the underlying resistance mechanisms. However, nanoscale or even near-atomic scale chemical mapping of cellular targets still remains a technological challenge, and advances could have immediate impacts on both fundamental and clinical research particularly for the fight against antibiotic resistance.

So far, several advanced microscopy and mass spectroscopy techniques have been applied to subcellular imaging. Transmission electron microscopy (TEM) has been a principal tool for investigating the ultrastructures of cells, and incorporation of a cryogenic environment allows high-resolution imaging of the cellular architectures in their near-native state.[3] The introduction of fluorescence probes and improved resolution
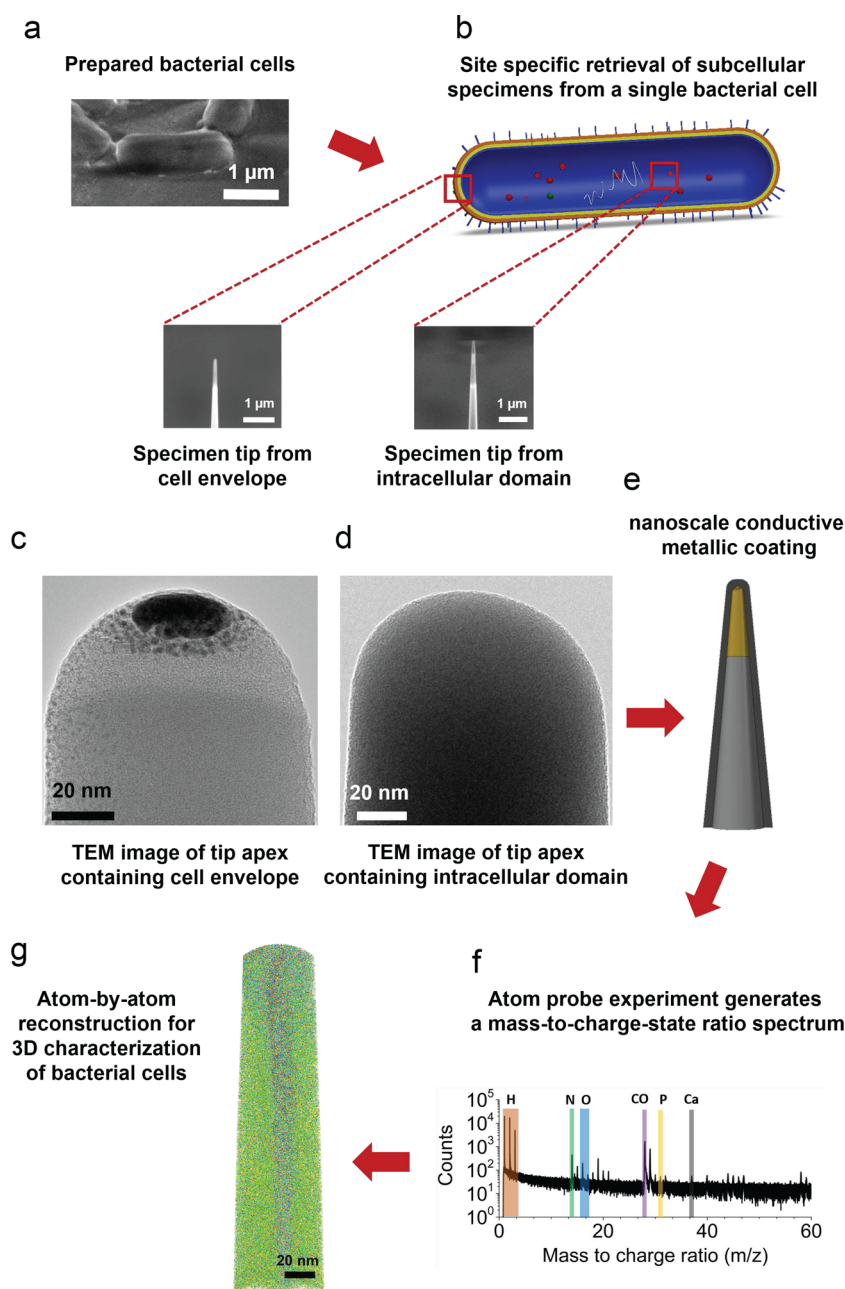
Figure 1. Schematic of the proposed approach for site-specific 3D atomic-scale analysis of bacterial cells. (a) A specimen from a single bacterial cells was retrieved using FIB-lift-out technique, and (b) a site-specific final needle-shaped specimen tip was achieved by precise annular FIB milling and contained a specific region of the original cell (either cell envelope or intracellular domain). (c−d) Selected site specific needle-shaped specimens from the cell envelope and intracellular domains were observed with conventional TEM. (e) Prior to APT, sufficient electrical conductivity is achieved with a nanoscale layer of metallic coating, which allows field evaporation of the specimen tip via pulsed-voltage APT and leads to (f) a mass-to-charge-state ratio spectrum of the ionic species followed by (g) an actual 3D reconstruction of the tomographic map at near-atomic resolution.

in light microscopy also provide an effective yet indirect approach to examine the spatiotemporal pattern of certain proteins in cells.[4,5] A recent cutting-edge biological imaging tool is atom probe tomography (APT), which has demonstrated a significant potential in achieving three-dimensional (3D), near-atomic resolution of biomaterials.[6,7] The principle of APT is well-established:[8,9] atoms are progressively removed from the surface of a cryogenically cooled, needle-shaped specimen under ultrahigh vacuum conditions by the process of field evaporation. Upon application of a high voltage to the specimen, a very intense electrostatic field is produced at the tip apex having a radius of curvature less than 100 nm, and by

using either voltage or laser pulsing (notably, the mechanism of field evaporation is different between the two pulsing modes: voltage pulsing increases the applied electric field, whereas laser pulsing increases the thermal energy to overcome the barrier to field ionization, and thereby trigger field evaporation) surface atoms are subsequently field ionized and evaporated toward a position-sensitive detector in a controlled manner. The chemical identity of each ion is determined by time-of-flight mass spectrometry (flight time from the tip apex to the detector), from which the mass-to-charge-state ratio is determined.[8,9] The mass-resolving power of the APT technique allows the detection of all of the atoms in the periodic table
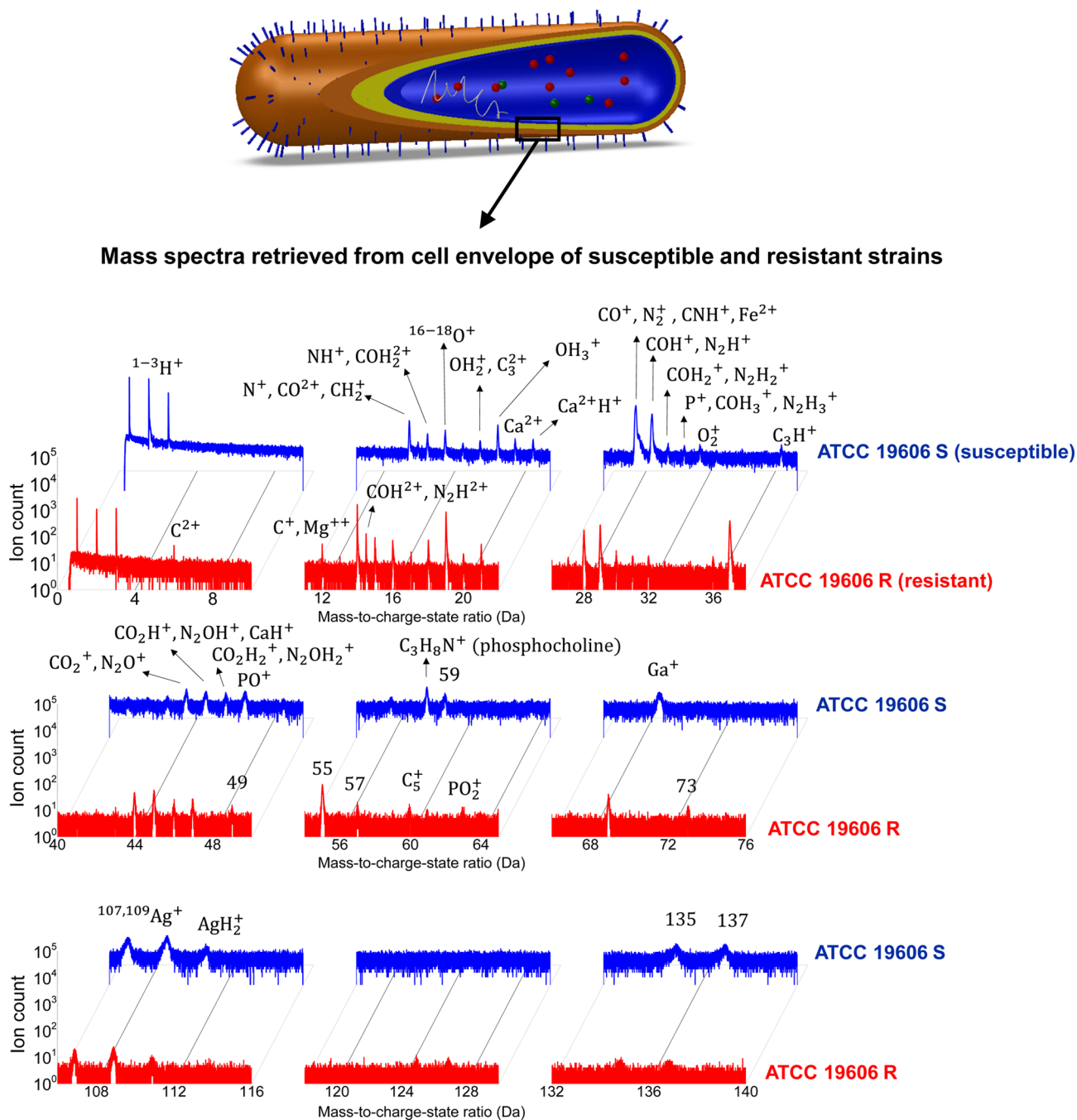
Figure 2. Mass-to-charge-state ratio spectra acquired from the cell envelope of *A. baumannii*, revealing distinct information from both a susceptible strain (ATCC 19606 S) highlighted in blue and a resistant strain (ATCC 19606 R) highlighted in red.

with equal sensitivity, including their individual isotopes, and in various ionic charge states. Following the atom probe experiment, to produce a tomographic data set, the evaporated volume is reconstructed in 3D using an inverse projection reconstruction algorithm and the sequence of detected events. The tomographic data set typically spans tens to hundreds of nanometers in depth and contains the spatial coordinates and elemental identities of tens to hundreds of millions of atoms with near atomic resolution ($\sim 0.1-0.3$ nm in depth and $0.3-0.5$ nm laterally).[10,11]

The nature of conventional pulsed-voltage APT requires the specimen to be analyzed to satisfy two criteria: (1) to conform to a needle-shaped tip with an end radius <100 nm and (2) to

possess sufficiently high electrical conductivity. For biological samples, the first challenge has been addressed with FIB-based "lift-out" approaches that were originally developed for TEM sample preparation[12] and have recently been utilized for specimen preparation of atomic force microscopy (AFM) to probe interior sections of biological materials.[13] After retrieval of the micron-sized "lift-out" sample from the bulk material, annular milling with low-current FIB is performed to gradually reduce the tip radius to the required size.[14] The conductivity requirement has been circumvented by the introduction of pulsed-laser APT to assist field evaporation at the tip surface. Using both FIB lift-out and laser-assisted APT, it has been demonstrated that 3D atomic imaging is feasible from a single
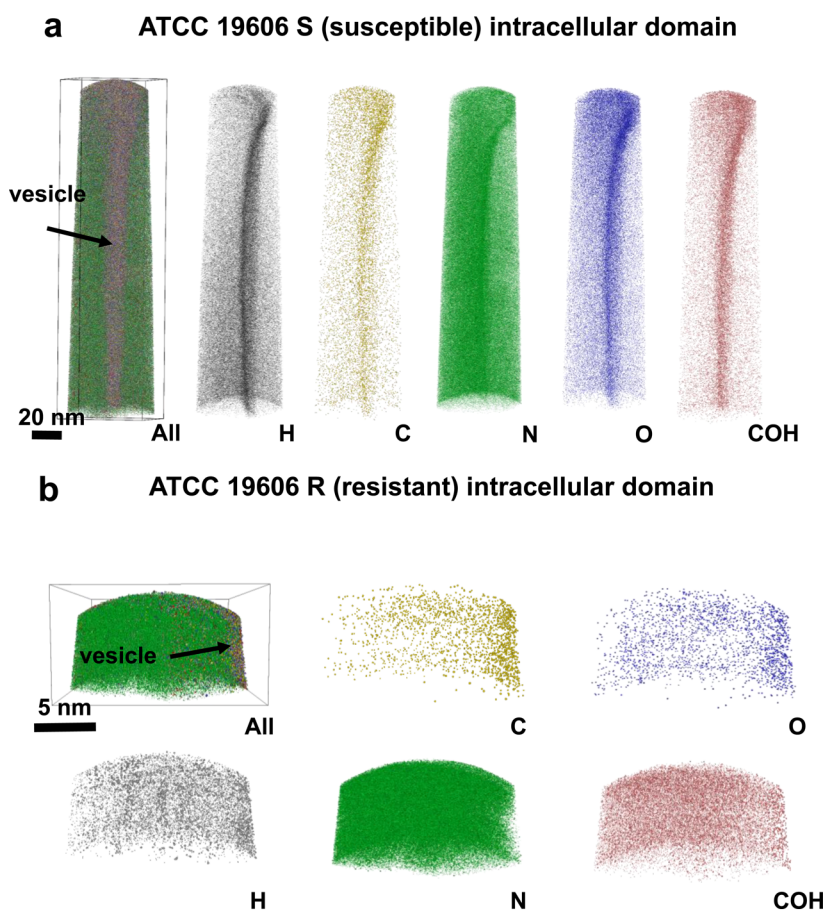
Figure 3. 3D ion species maps from the APT reconstructions of (a) intracellular domain of a susceptible strain and (b) intracellular domain of a resistant strain.

mammalian cell (e.g., HeLa cell).[15] However, there exists a well-known challenge of optimizing the laser parameters, namely, laser duration, wavelength, and energy, which collectively can contribute to spatial and compositional errors.[16,17] Furthermore, since organic molecules tend to undergo structural phase transitions at much lower temperatures relative to inorganic materials, thermally induced field evaporation of organic materials using a pulsed laser is much more sensitive to these operational parameters and can result in poorer spatial resolution.[18]

As an alternative to laser pulsing of an electrically insulated target, it has been hypothesized that sufficient field evaporation can be achieved in pulsed-voltage APT in the presence of a thin, conductive coating layer on the specimen.[18] In previous studies, numerical simulations of voltage distribution in both uncoated and coated bacterial cell APT specimens have been performed, using physical data relating to bacterial cells found in the literature. The simulation results suggested that, given a conductive shell of thickness 10 nm or more, a remarkable uniform voltage distribution throughout the specimen can be achieved, which is desirable for pulsed-voltage APT study of biological specimens.[19] In contrast, a significantly nonuniform voltage distribution was found on an equivalent uncoated cell specimen.

A schematic diagram of the proposed approach adopted in the present study is presented in Figure 1. The intracellular domain and cell envelope samples retrieved from the target bacterial cell were fabricated into needle-shape specimens suitable for APT using well-established FIB lift-out technique,[20,21] followed by application of a nanoscale conductive metallic coating prior to the APT experiments. Key steps of sample preparation are presented in the Figure 1a−d, and the complete protocol is provided in Supporting Information (Supporting Figure 1). In parallel, aliquots of the bacterial strains were also imaged by cryo-TEM, which allowed the ultrastructure to be investigated in the near-native state and provides invaluable insights for interpreting the APT data. Prior to the atom probe experiments, selected specimens were also imaged by SEM and TEM (Figure 1c,d) to verify site-specific sample preparation from the cell envelope and intracellular domains of target bacterial cells.

In this APT study, the areas of interest include the intracellular and cell envelope regions of polymyxin-susceptible and resistant strains of *A. baumannii*. Figure 2 demonstrates the acquired mass-to-charge-state ratio spectra for the cell envelope region. Also, the mass spectra for the intracellular domain of polymyxin-susceptible and -resistant strains of *A. baumannii* are presented in the Supporting Information (Supporting Figure 2). Assignment of the peaks to ionic species is nontrivial, as is the case for APT spectra from most organic material,[6,15,24] given the number of peaks and also the propensity for detection of both atomic and molecular ions in various charge states, such that peak overlap between ionic species can easily occur.[6,15,22] Considering the regions of interest and their possible compositions from the available literature, the peak assignments presented in the Figure 2 represent the best possible matches.

Peaks for Ga$^+$ and Ga^{2+} (69 and 34.5 Da, respectively), a typical artifact caused by implantation during FIB sample preparation, were present, but the amount of Ga implantation is limited in all spectra (average concentration from 0.9 to 2.24%). Also, peaks corresponding to Ag$^+$, the conductive coating material used in the sputter coating process, were detected at 107 and 109 Da, where the source could either be the coating layer itself or Ag atoms that have migrated into the cellular specimens during coating. 1D average atomic concentration (%) profile of Ag along the length of the tomographic reconstructions (z-axis) showed that Ag concentration at the tip apex was relatively higher. After the cellular region was exposed to the field after the removal of the Ag coating layer, the concentration of Ag significantly decreased as expected (Supporting Figure 3). These two atom types (Ga and Ag), however, represented only a minor fraction of the collected ions from the total composition of the intracellular and cell envelope data (in the cell envelope, 1.12% Ga and 2.73% Ag detected in polymyxin-susceptible strain (ATCC 19606 S); and 1.3% Ga and 1.41% Ag in the resistant strain (ATCC 19606 R); for specimens from intracellular domain, 2.24% Ga and 0.76% Ag from ATCC 19606 S and 0.9% Ga and 0.29% Ag from ATCC 19606 R). It is rational to exclude Ag and Ga from further analysis as neither element is considered to be present in native biological cells. Similarly, it should be noted that, while hydrogen was detected in the current APT experiments and could be expected to occur in molecular species such as hydroxyl and carbonyl groups, some fraction is likely due to remnant H atoms in the vacuum chamber of the atom probe instrument. It is well-known that this small atom is notoriously difficult to remove, even from ultrahigh vacuum systems.[23] This serves to make the exact peak assignment within the mass spectrum more challenging. However, a comparison of the mass spectra retrieved from the intracellular domain of mammalian cells using pulsed-laser APT[15] with the current intracellular bacterial APT data shows that there are peaks in common, including ^{12}C$^+$ (12 Da), ^{14}N$^+$ (14 Da), ^{16}O$^+$ (16 Da), and H$_2$O$^+$ (18 Da). Notably, there is also a peak at 28 Da, with potential candidates including the carbonyl group (CO$^+$) and N$_2^+$. This particular ion was found in all cellular specimens but was more pronounced in the mammalian cell[15] and bacterial cell envelope. In the present study, the peak at 28 Da was designated as CO, although the chance of partial involvement of N$_2$ could not be excluded.

Runs containing 1−2 million ions were routinely recorded in the present study, and long structural features, 5−10 nm wide running through the tomographic reconstructions of the intracellular domains of both polymyxin-susceptible and resistant strains, have been observed (Figure 3a−b). Although only indirectly supported by complementary cryo-TEM images (Figure 4a−d), these long structural features were likely the membrane of the intracellular vesicles. A one-dimensional (1D) composition profile across these band/interface-like features suggests that they are rich in C, O, H, and COH and could therefore be part of an energy storage region.

The atom probe data acquired from cell envelope, on the other hand, displayed more complicated 3D structural forms that resemble network/fibril features (Figure 5a-b). A distinct peak at 31 Da, relating to phosphorus (P), was detected in the cell envelope but not pronounced in the intracellular specimen (Figure 2 and Supporting Figure 2). 1D concentration profiles of the network arms observed in the cell envelope specimen revealed band regions in the order of 5−10 nm with
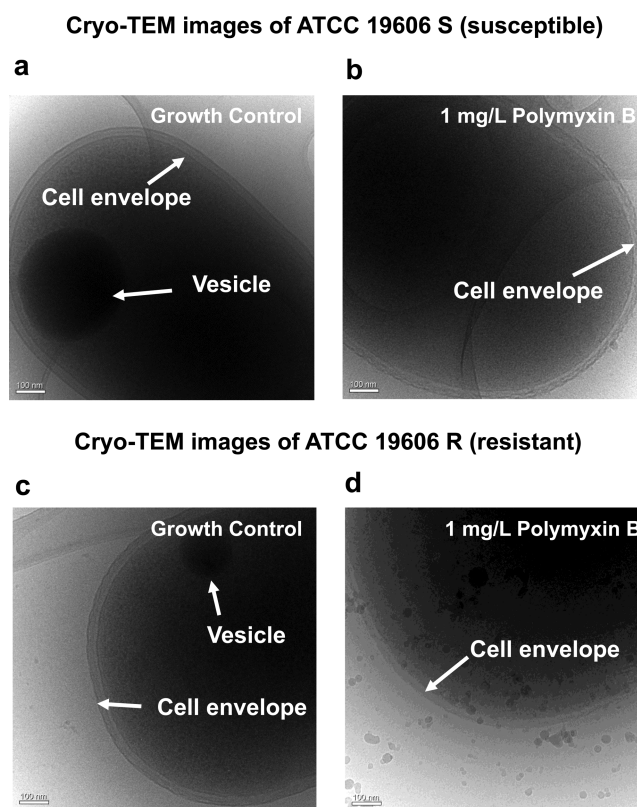
Cryo-TEM images of ATCC 19606 S (susceptible)

Cryo-TEM images of ATCC 19606 R (resistant)

Figure 4. Cryo-TEM images of the cell envelope from (a) control and (b) polymyxin B treated *A. baumannii* susceptible strain (ATCC19606 S) and from the control and polymyxin B treated resistant strain (ATCC19606 R) in (c) and (d), respectively.

significantly elevated concentrations of C and O. Moreover, a peak at 58 Da was detected in the cell envelope of the polymyxin-susceptible strain. The 58 Da species was not present in the intracellular specimens of the both bacterial strains in the current work, nor in the mammalian cell study by Narayan et al.[15] In addition, 58 Da was also below the detection limit in the polymyxin-resistant strain. In the time-of-flight secondary ion mass spectrometry (TOF-SIMS) imaging of *Xenopus laevis* oocytes using C$_{60}^+$ (Buckminsterfullerene) primary ions, it has been reported that a peak at m/z value of 58 was attributed to a fragment of phosphocholine (C$_5$H$_{15}$NO$_4$P).[24] Considering the region where the data were collected (cell envelope) and given the fact that the elements C, H, N, O and P have also been observed in the mass spectrum, the peak at 58 Da in the APT mass spectrum from the polymyxin-susceptible bacterial cell envelope likely represents a phosphocholine fragment (C$_3$H$_8$N$^+$).[24,25] As such, the band region in the bottom-left area of the tomogram in Figure 5a (58 Da) detected in this study is considered as a candidate for the phospholipid bilayer.[24,25]

On the basis of the literature,[26,27] it has been hypothesized that in *A. baumannii* polymyxin, resistance occurs due to the loss of the initial binding target, the lipid A component of lipopolysaccharide (LPS). A comparison of the data obtained from the cell envelope of polymyxin-susceptible and resistant strains reveals the presence of phosphocholine fragments only in the cell envelope of polymyxin-susceptible strain, which suggests loss or damage of the lipid layers of the polymyxin-resistant cells. Also, colocalization of species (59, 135, 137, 163, and 165 Da) was observed within the cell envelope of the
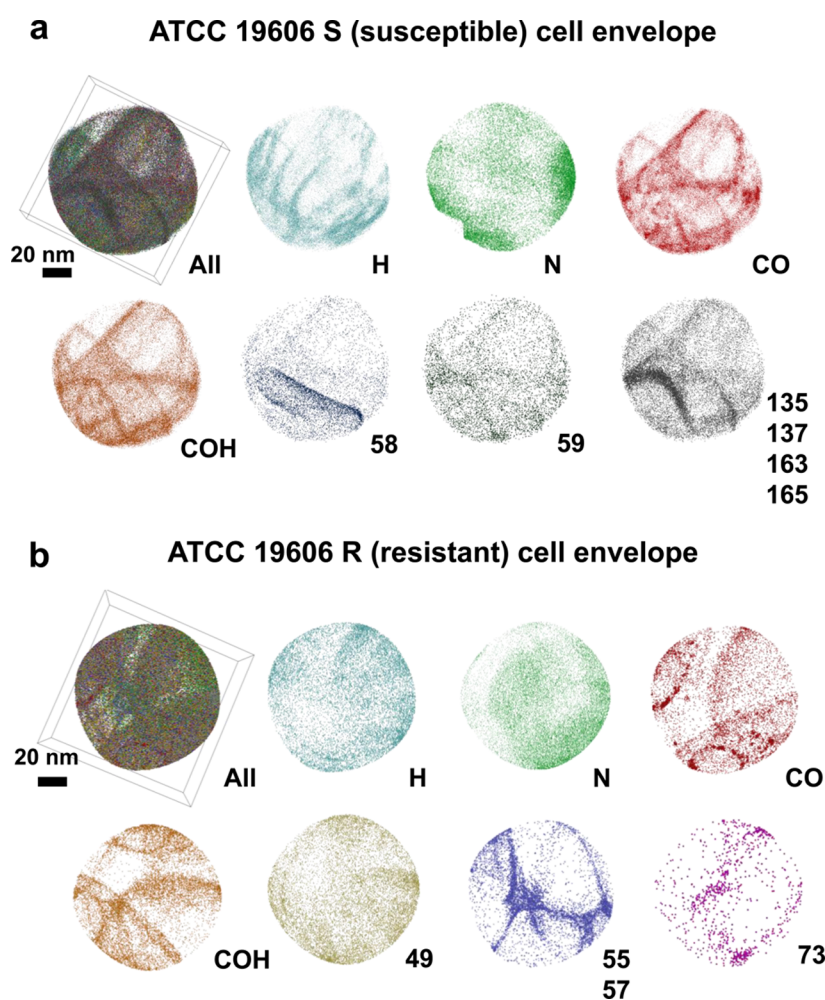
Figure 5. 3D ion species maps from the APT reconstructions of (a) cell envelope of susceptible strain, and (b) cell envelope of resistant strain.

polymyxin-susceptible strain (Figure 5a), which implies that these peaks represent fragments of the same molecule possibly related to lipids.[28,29]

It should be highlighted that previous knowledge regarding changes of the bacterial envelope due to drug resistance was primarily hypothesized based on bulk analysis data, while our current data provide the first direct imaging of the corresponding molecules in situ. Repeat mass-to-charge-state ratio spectra (Supporting Figures 4–7) were also collected to confirm the consistency of the above-mentioned results and reinforce the interpretations made. These data also confirm the repeatability of the pulsed-voltage APT method for analysis of nonconducting biological material, and agreement between the replicates for all four cases greatly strengthens the validity of the work that was performed.

Although the work presented here is an important step toward adopting APT for biological analysis, there are indeed some limitations that should be discussed. Notwithstanding the fact that APT has extraordinary capabilities in terms of mass and spatial resolution as demonstrated in this study, the field-of-view or volume of analysis is extremely small which inherently imposes restrictions on the translation of the results into statistical meaningful information. From a sample preparation point of view, while the in situ sample preparation challenge has been addressed with the FIB lift-out approach, precise retrieval and positioning of nanoscale biological targets at the tip apex are very time-consuming. Moreover, for a successful APT study of biological cells, dehydration is recommended in order to avoid the possibility of cell destruction.[15] Although it has been previously shown that proper protocols can be utilized for cell sample preparation to limit the impact on the structure and chemical composition of the cells,[15,30,31] it should also be noted that perturbations in chemical mapping of dehydrated specimens cannot be completely avoided.[15] Nevertheless, the proposed approach in this study will remain as a promising solution until the successful development of cryo-transfer of cryo-fixed samples into the APT instrument. Further challenges include understanding the complexities in the probing/imaging process, with respect to field evaporation of biological molecules on the tip apex in the pulsed-voltage mode. Similarly, laser−matter interaction of biological material under thermal field evaporation in the pulsed-laser mode requires further investigations.[18,22,32,33] Finally, since APT is a relatively new technique for biological materials, establishing protocols for confident peak identification in the mass spectrum is essential for accurate elemental composition analysis of the acquired data.

In conclusion, successful APT experiments have been performed on bacterial cell specimens prepared by a FIB lift-out approach and subsequently coated with a nanoscale layer of Ag. These results show that, even without pulsed-laser acquisition, 10^6−10^7 ions can be collected from coated bacterial cell specimens compared to only 10^3−10^4 ions from uncoated control specimens (Supporting Figure 8). Mass spectra and

reconstructed 3D data volumes were obtained from both the intracellular domain and cell envelope regions, while damage from sample preparation, namely, Ga^+ ion implantation, was minimal. The application to explore the drug resistant pathogens highlighted the capabilities of the proposed APT method. The distinct mass spectra from polymyxin-susceptible and resistant strains, primarily at the cell envelope, shed light on the compositional changes involved in the development of polymyxin-resistant mechanisms, which were not possible to be imaged in situ in previous studies. We expect the experimental approach demonstrated in this work will significantly contribute into the future as a tool to investigate the architecture and chemistry of biological cells at the atomic-scale resolution.

Materials and Methods. *Bacterial Cell Sample Preparation.* Colonies of *A. baumannii*, both susceptible (ATCC 19606 S) and resistant (ATCC 19606 R) to polymyxin B (from ATCC), were inoculated into cation-adjusted Mueller-Hinton broth (CAMHB). Overnight cultures were incubated in a shaking water bath for 18 h. Log-phase cultures were prepared by inoculating 1:100 of overnight culture into CAMHB and incubated for 3.5 h. Also, sterile 1 mg/mL solution of polymyxin B sulfate was prepared using Milli-Q water and a 0.22 μm syringe filter. Samples were washed 3 times in phosphate buffered saline (PBS), then fixed in 4% paraformaldehyde in PBS for 20 min. For each sample, 10 μL of the suspension was added onto silicon nitride membranes, and the samples were air-dried in a biosafety cabinet.

The bacterial cells were subsequently transferred to a FIB-SEM instrument (Quanta 3D FEG, FEI Company) for initial scanning electron microscopy (SEM) inspection at low voltage (~1 kV). After selection of a single cell, APT specimen preparation was performed using the "lift-out" approach and a chamber-installed micromanipulator (MM3A-EM, Kleindiek Nanotechnik GmbH), with detailed steps presented in the Supporting Information (Supporting Figure 1). After successful lift-out, FIB annular milling was performed with decreasing inner and outer diameters associated with decreasing current–voltage parameters in order to achieve the tip radius required for APT. The radii of the final needle-shaped specimens containing cellular material ranged from 60 to 110 nm.

Sputter Coating Experiments. Sputter coatings were carried out using a high-resolution sputter coater (Cressington 208 HR Sputter Coater, Cressington Scientific Instruments Inc.) equipped with a Ag target. Imaging of coated tips was performed using a SEM instrument (Nova NanoSEM 450 FEG SEM, FEI Company). Secondary electron (SE) imaging was carried out in immersion mode with a 2 kV voltage and nominal probe current of 14 pA, and imaging of the end tips was performed with tilt angle of 52°.

Transmission Electron Microscopy. High-resolution imaging of the biological tips prepared for APT was performed using TEM (Tecnai G2 F20, FEI Company) with accelerating voltage at 200 kV. For TEM sample preparation of coated APT tips, a FIB lift-out approach with a micromanipulator (MM3A-EM, Kleindiek Nanotechnik GmbH) was performed to attach the coated APT specimens on the TEM grid with Pt gas deposition. The conventional plunge freezing method was also utilized for cryo-TEM imaging of the bacterial strains of interest. The cells (suspended in the PBS medium) were transferred onto a TEM grid followed by blotting using a specialized paper (Waterman, 3M). These samples were then rapidly immobilized in liquid nitrogen cooled by liquid ethane, followed by transfer into the TEM with a cryo-sample holder.

Atom Probe Tomography. APT measurements were conducted using a local electrode atom probe (LEAP 4000 HR, Cameca Instruments) in pulsed-voltage mode. Experiments were performed with a voltage pulse repetition rate of 200 kHz, pulse fraction (ratio of the pulse voltage to the DC standing voltage) of 20%, detection rate of 0.5% (0.005 ions/pulse), and specimen temperature of ~60 K. Reconstruction and visualization of the APT data was performed using IVAS 3.6.12 software (Cameca Instruments). To consider the volume of undetected atoms, a detector efficiency of ~42% as quoted by the manufacturer was considered in the tomographic reconstruction steps. Further data visualization was performed using the commercial software, Avizo 8.1.0 Fire (FEI Company).

■ ASSOCIATED CONTENT

Ⓢ Supporting Information

The Supporting Information is available free of charge on the ACS Publications website at DOI: 10.1021/acs.nanolett.6b03409.

> Details regarding FIB lift-out APT sample preparation from bacterial cells (Supporting Figure 1), mass-to-charge-state spectra acquired from intracellular domains of susceptible and resistant strains of *A. baumannii* (Supporting Figure 2), 1D atomic concentration (%) profile of Ag along the *z*-axis of the tomographic reconstruction (Supporting Figure 3), repeats of mass-to-charge-state ratio spectra collected from APT experiments along with corresponding images of the specimen tips before and after probing (Supporting Figures 4−7), and application of metallic coating for APT specimen preparation from bacterial cells (Supporting Figure 8) (PDF)

■ AUTHOR INFORMATION

Corresponding Author

*E-mail: jing.fu@monash.edu. Fax: 61-3-99051825.

Notes

The authors declare no competing financial interest.

■ ACKNOWLEDGMENTS

■ REFERENCES

(1) The Review on Antimicrobial Resistance, Final report; http://amr-review.org/Publications (accessed May 18, 2016).

(2) Walsh, C. *Nature* **2000**, *406* (6797), 775−781.

(3) Dubochet, J.; Al-Amoudi, A.; Bouchet-Marquis, C.; Eltsov, M.; Zuber, B. CEMOVIS: cryo-electron microscopy of vitreous sections. In *Handbook of Cryo-preparation Methods for Electron Microscopy*; Cavalier, A., Spehner, D., Humbel, B. M., Eds.; CRC Press: Boca Raton, FL, 2009; pp 259−289.

(4) Fernandez-Suarez, M.; Ting, A. Y. *Nat. Rev. Mol. Cell Biol.* **2008**, *9* (12), 929−943.

(5) Huang, B.; Wang, W.; Bates, M.; Zhuang, X. *Science* **2008**, *319* (5864), 810−813.

(6) Gordon, L. M.; Joester, D. *Nature* **2011**, *469* (7329), 194−197.

(7) Gordon, L. M.; Joester, D. *Front. Physiol.* **2015**, *6*, 57.

(8) Gault, B.; Moody, M. P.; Cairney, J. M.; Ringer, S. P. *Atom probe microscopy*; Springer Science & Business Media: New York, 2012; Vol. 160.

(9) Miller, M. K.; Forbes, R. G. *Atom-Probe Tomography: The Local Electrode Atom Probe*; Springer Science and Business Media: New York, 2014.

(10) Cadel, E.; Vurpillot, F.; Lardé, R.; Duguay, S.; Deconihout, B. *J. Appl. Phys.* **2009**, *106* (4), 044908.

(11) Gault, B.; Moody, M. P.; de Geuser, F.; Haley, D.; Stephenson, L. T.; Ringer, S. P. *Appl. Phys. Lett.* **2009**, *95* (3), 034103.

(12) Giannuzzi, L. A.; Stevie, F. A. *Micron* **1999**, *30* (3), 197−204.

(13) Adineh, V. R.; Liu, B.; Rajan, R.; Yan, W.; Fu, J. *Acta Biomater.* **2015**, *21* (0), 132−141.

(14) Miller, M. K.; Russell, K. F.; Thompson, K.; Alvis, R.; Larson, D. J. *Microsc. Microanal.* **2007**, *13* (06), 428−436.

(15) Narayan, K.; Prosa, T. J.; Fu, J.; Kelly, T. F.; Subramaniam, S. *J. Struct. Biol.* **2012**, *178* (2), 98−107.

(16) Bunton, J. H.; Olson, J. D.; Lenz, D. R.; Kelly, T. F. *Microsc. Microanal.* **2007**, *13* (06), 418−427.

(17) Gault, B.; La Fontaine, A.; Moody, M. P.; Ringer, S. P.; Marquis, E. A. *Ultramicroscopy* **2010**, *110* (9), 1215−1222.

(18) Kelly, T. F.; Nishikawa, O.; Panitz, J. A.; Prosa, T. J. *MRS Bull.* **2009**, *34* (10), 744−750.

(19) Adineh, V. R.; Marceau, R. K. W.; Chen, Y.; Si, K. J.; Velkov, T.; Cheng, W.; Jian, L.; Fu, J. Chemical mapping of biological materials using pulsed-voltage atom probe tomography, under Review.

(20) Miller, M. K.; Russell, K. F.; Thompson, G. B. *Ultramicroscopy* **2005**, *102* (4), 287−298.

(21) Thompson, K.; Lawrence, D.; Larson, D. J.; Olson, J. D.; Kelly, T. F.; Gorman, B. *Ultramicroscopy* **2007**, *107* (2−3), 131−139.

(22) Greene, M. E.; Kelly, T. F.; Larson, D. J.; Prosa, T. J. *J. Microsc.* **2012**, *247* (3), 288−299.

(23) Sundell, G.; Thuvander, M.; Andrén, H. O. *Ultramicroscopy* **2013**, *132*, 285−289.

(24) Fletcher, J. S.; Lockyer, N. P.; Vaidyanathan, S.; Vickerman, J. C. *Anal. Chem.* **2007**, *79* (6), 2199−2206.

(25) Brison, J.; Robinson, M. A.; Benoit, D. S.; Muramoto, S.; Stayton, P. S.; Castner, D. G. *Anal. Chem.* **2013**, *85* (22), 10869−10877.

(26) Henry, R.; Vithanage, N.; Harrison, P.; Seemann, T.; Coutts, S.; Moffatt, J. H.; Nation, R. L.; Li, J.; Harper, M.; Adler, B. *Antimicrob. Agents Chemother.* **2012**, *56*, 59−69 AAC..

(27) Azad, M. A.; Finnin, B. A.; Poudyal, A.; Davis, K.; Li, J.; Hill, P. A.; Nation, R. L.; Velkov, T. *Antimicrob. Agents Chemother.* **2013**, *57*, 4329.

(28) Passarelli, M. K.; Winograd, N. *Biochim. Biophys. Acta, Mol. Cell Biol. Lipids* **2011**, *1811* (11), 976−990.

(29) Fletcher, J. S.; Vickerman, J. C.; Winograd, N. *Curr. Opin. Chem. Biol.* **2011**, *15* (5), 733−740.

(30) Szakal, C.; Narayan, K.; Fu, J.; Lefman, J.; Subramaniam, S. *Anal. Chem.* **2011**, *83* (4), 1207−1213.

(31) Porter, K.; Anderson, K. *Eur. J. Cell Biol.* **1982**, *29* (1), 83−96.

(32) Panitz, J. A. In *Prospects for Atom-Probe Analysis in Biology and Medicine*, Proc. 52nd Annual Meeting of the Microscope Society of America, San Francisco, CA, USA, 1994; Bailey, G. W., Garratt-Reed, A. J., Eds.; San Francisco Press: San Francisco, CA; pp 824−825.

(33) Braet, F.; Soon, L.; Kelly, T. F.; Larson, D. J.; Ringer, S. P. Some new advances and challenges in biological and biomedical materials characterization. In *Nanotechnologies for the Life Sciences*; John Wiley and Sons, Inc.: Sept 15, 2007; pp 292−318.